Organic Electronics 66 (2019) 116–125

Contents lists available at ScienceDirect

Organic Electronics

journal homepage: www.elsevier.com/locate/orgel

Effect of surface morphology of slot-die heads on roll-to-roll coatings of fine PEDOT:PSS stripes

Gi-Eun Kim, Dong-Kyun Shin, Jin-Young Lee, Jongwoon Park*

School of Electrical, Electronics & Communication Engineering, Korea University of Technology and Education, Cheonan, 330-708, South Korea

ARTICLE INFO

Keywords:
Slot-die head
Surface morphology
Meniscus guide
μ-tips
Fluid dynamics

ABSTRACT

One of key components in the roll-to-roll slot-die coating system for the fabrication of fine stripes using poly(3,4-ethylenedioxythiophene):poly(4-styrenesulfonate) (PEDOT:PSS) aqueous solution is the slot-die head with a shim and meniscus guide embedded together. We have fabricated the meniscus guide with 150-μm-wide μ-tips using an easily processable film for potential application in solution-based organic light-emitting diodes (OLEDs) displays. However, the success or failure of fine stripe coatings is shown to depend sensitively on the surface morphology of slot-die heads. We have investigated the coating behaviors of two slot-die heads with different surface morphology by changing the configurations of the shim and meniscus guide. Using the slot-die head with good surface roughness but local scratches, it is not feasible to fabricate 100 stripes within the effective coating width of 150 mm. We have demonstrated through computational fluid dynamics (CFD) simulations that the continuous fluid flow is interrupted and thus the fluid velocity is reduced in the presence of scratches, a phenomenon related to coating defects (line breakup and merging). Using the slot-die head with uniformly rough surface but no scratches, however, we can fabricate 150 stripes without defects by reducing the μ-tip length and the shim thickness. It is observed that the inter-stripe width and thickness uniformities are degraded with increasing number of stripes due to the degraded uniformity of the pressure distribution inside the cavity (ink distribution chamber). Finally, we have fabricated OLEDs on the conductive PEDOT:PSS stripes and successfully achieved light emission from 125 OLED stripes.

1. Introduction

Solution processes for the fabrication of organic thin films offer great potential for achieving low-cost manufacturing of large-area organic light-emitting diode (OLED) display panels. Coating methods (e.g., slot, spin, spray, blade, etc.) are preferred for full-area coatings of the common layers of OLEDs [1–7]. Meanwhile, printing methods (e.g., inkjet, nozzle, gravure, offset, etc.) are suitable for the formation of RGB pixels requiring lateral and/or longitudinal patterning [8]. Lately, a hybrid solution method (nozzle printing for RGB stripes and slot-die coating for blanket layers) was employed to fabricate active-matrix OLED (AMOLED) display panels [9,10]. Such a hybrid process was inevitably used because RGB stripe coating was not readily feasible by slot-die coating. Stripe coating for RGB pixels offers an approach to remove the pixel bank structure used to confine ink droplets [11–13]. In fact, slot-die coating was employed to fabricate stripe-patterned polymer solar cells [1]. It requires a slot-die head with not only a shim mask defining the feed slot width but also a meniscus guide with small protrusion. The meniscus guide is protruded from the die lip such that the meniscus is formed between the meniscus guide and substrate, thereby preventing the joining of the menisci between two adjacent stripes [14,15]. Such a slot-die head with the meniscus guide has been used to fabricate wide stripes (centimeters in width) required for solar cells. For display applications, however, highly uniform coatings of fine stripes as narrow as pixels (~100 μm) and as dense as a pixel array should be feasible. It entails micropatterning of a thin (20 μm–100 μm) stainless steel used for the shim and meniscus guide. Even with a high precision process machine, it is very difficult to implement micropatterning of the meniscus guide with small protrusions (μ-tips) as narrow as pixels. In this work, we fabricate both a shim mask and a meniscus guide with multiple μ-tips using an easily processable film and employ them to fabricate fine stripes of poly(3,4-ethylenedioxythiophene):poly(4-styrenesulfonate) (PEDOT:PSS).

In slot coating of fine PEDOT:PSS stripes using the shim and meniscus guide with μ-tips, however, the fluid dynamics through slit channels would be affected by some defects (e.g., scratches on the surface, rough surfaces, curved surfaces, etc.) that may exist in slot-die heads because the quantity of fluid flowing through each slit channel

* Corresponding author.
E-mail address: pjwup@koreatech.ac.kr (J. Park).

https://doi.org/10.1016/j.orgel.2018.12.033
Received 4 October 2018; Received in revised form 14 December 2018; Accepted 18 December 2018
Available online 20 December 2018

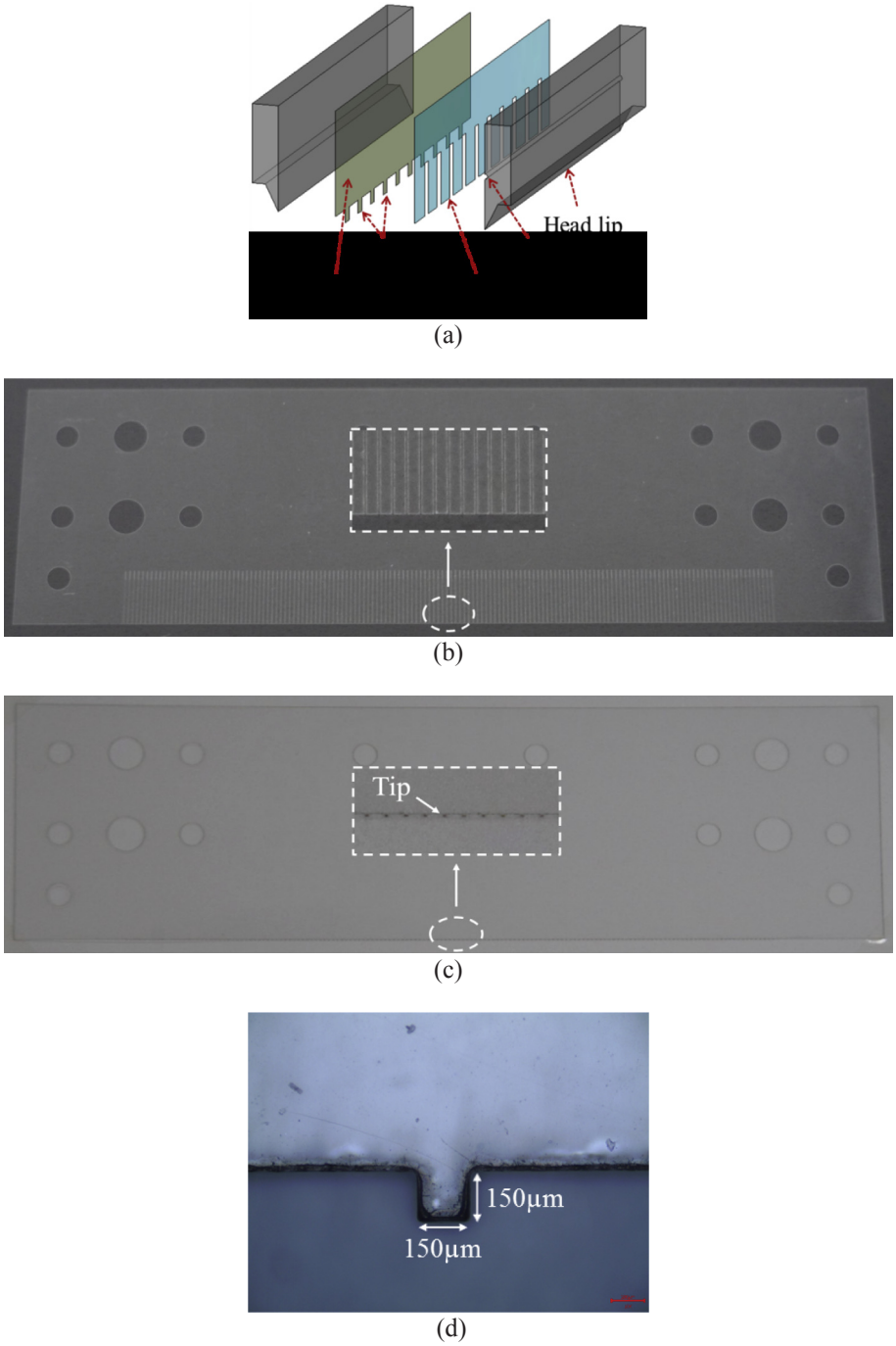

Fig. 1. (a) Schematic view of slot-die head used for fine stripe coatings, (b) image of a shim with 150 slit channels fabricated using 25-μm-thick PET film, (c) a meniscus guide with 150 μ-tips fabricated using 188-μm-thick PET film, and (d) magnified image of a 150-μm-wide and 150-μm-long tip.

Table 1
Summary of process variables and configurations of slot head components.

Parameters	25 stripes	50 stripes	100 stripes	150 stripes
Flow rate (ml/min)	0.025	0.05	0.1	0.15
Coating gap (μm)	20			
Shim thickness (μm)	50	50	25/50/100	25
Meniscus guide thickness (μm)	188			
μ-Tip width (μm)	150			
μ-Tip length (μm)	500	500	250/500	150
Distance between μ-tips (μm)	6000	2900	1350	850
Drying	80 °C/20 min.			

(outlet) is extremely small. It brings in coating defects such as line breakup and line merging. Therefore, it is highly demanded to employ the slot-die head with excellent surface morphology. To enhance it, surface polishing is required several times, increasing the manufacturing cost. Even so, the surface of the slot-die head is easily scratched during assembly, disassembly, and cleaning. More seriously, there would exist some tiny scratches that are invisible to the naked eye. As such, an investigation into the effect of its surface morphology on roll-to-roll slot coatings of fine PEDOT:PSS stripes deserves to be made. To this end, we employ two slot-die heads with the same configuration but different surface morphology and analyze their coating behaviors by changing the configurations of the shim and meniscus guide. It is addressed that compared to the slot-die head with good surface roughness

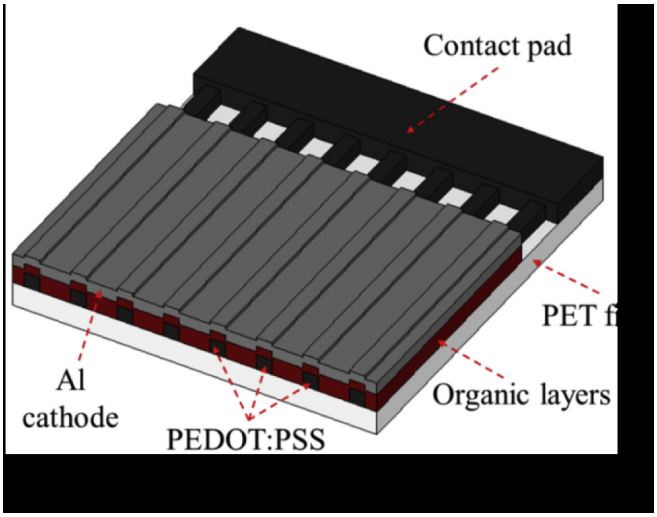

(a)

(b)

Fig. 2. (a) Schematic view of layer structure for the fabrication of OLED stripes and (b) layer structure of phosphorescent green OLED device.

but local scratches, the slot-die head with uniformly rough surface but no scratches shows more stable coating behaviors, especially when the number of stripes is high. To visualize the effect of minute scratches on the fluid dynamics in slit channels, we also perform 2D computational fluid dynamics (CFD) simulations. It is demonstrated that a large change in the transient phase distribution occurs in the presence of scratches, a phenomenon directly related to coating defects.

2. Methods

2.1. Experiment method

Presented in Fig. 1(a) is the schematic layout of a slot-die head employed for fine stripe coatings. In the slot-die head, both a shim for slit channels and a meniscus guide with μ-tips are embedded. Those μ-tips are protruded from the die lip in such a way that the meniscus is formed between the μ-tips and substrate. Two slot-die heads with the same configuration but different surface morphology were used for experiments. One slot-die head (Head A) has good surface roughness but local scratches on the surface, whereas the other slot-die head (Head B) does not have any scratch on the surface but uniformly rough

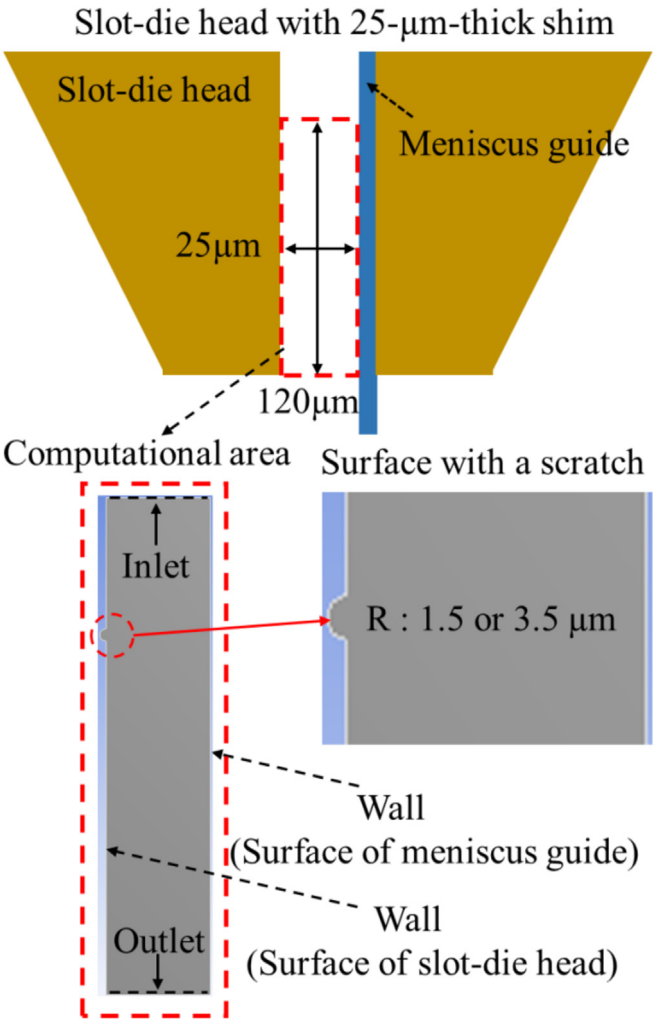

Fig. 3. Illustration of computational area (25 μm × 120 μm) with a scratch for 2D CFD simulations.

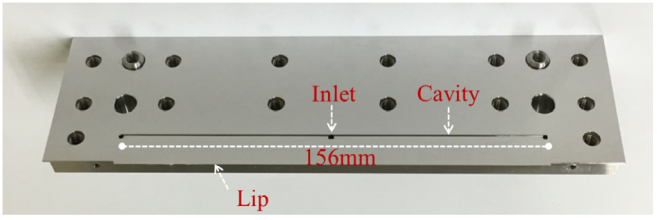

Fig. 4. Image of the inner surface of slot-die head with 156-mm-long and 2-mm-wide cavity (ink distribution chamber) and inlet located in the middle of the cavity.

surface over the entire plate. We analyzed the coating behaviors of those slot-die heads by changing the shim thickness, μ-tip length, and the number of μ-tips. The slot head configurations and process variables are summarized in Table 1. The flow rate was increased in proportion to the number of stripes (μ-tips) [16]. For both the shim and the meniscus guide, we used a polyethylene terephthalate (PET) film, which was readily processed using a laser cutting system (SPD-2000U, EO Technics). The shim fabricated to have 150 slit channels in a comb pattern and the meniscus guide with 150 μ-tips are shown in Fig. 1(b) and (c), respectively. As evident in Fig. 1(d), those μ-tips in Fig. 1(c) have the length of 150 μm and width of 150 μm. Stripe coatings were performed using a R2R slot coater that consists of a slot head module (head size: 200 mm × 30 mm × 58 mm, cavity (ink distribution chamber):

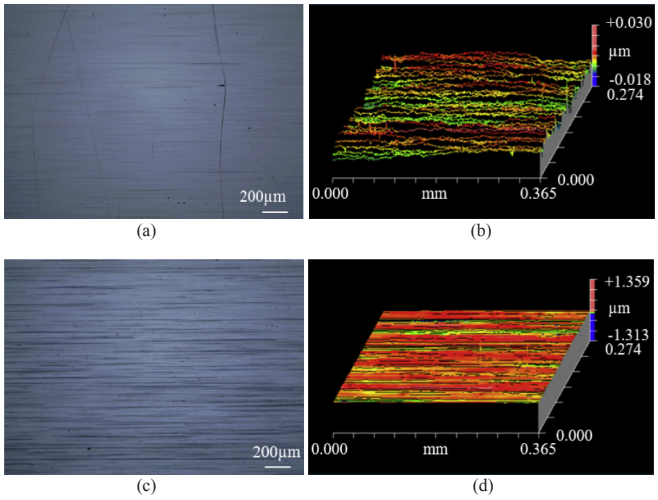

(a) (b) (c) (d)

Fig. 5. (a) Optical image of the surface of Head A with scratches, (b) its measured surface profile, (c) optical image of the surface of Head B without scratches, and (d) its measured surface profile.

Table 2
Surface roughness values of those slot-die heads measured at 8 points on the body surface.

Head A			Head B		
Surface with no scratches					
R_{pv} (μm)	R_{rms} (nm)	R_a (nm)	R_{pv} (μm)	R_{rms} (nm)	R_a (nm)
0.05	4.2	3.4	2.6	46	21
0.06	4.8	3.6	2.9	29	17
0.05	4.7	3.8	2.6	54	23
0.06	4.7	3.6	2.6	44	23
0.07	4.6	3.7	3.2	65	26
Surface with scratches					
3.5	76	19	No scratches		
2.3	37	7.9			
2.3	42	13			

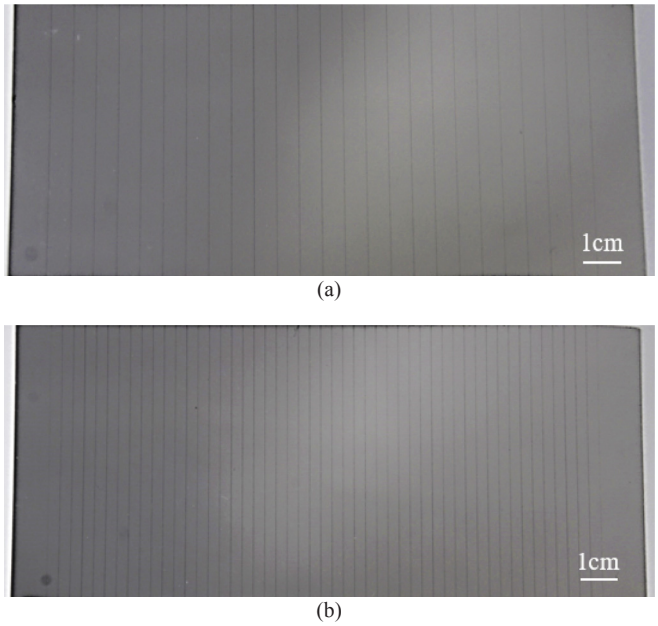

(a) (b)

Fig. 6. Images of (a) 25 stripes and (b) 50 stripes coated using Head B at the maximum coating speed of 20 mm/s under the process condition in Table 1.

Table 3
Measured width, thickness, and uniformity of 25 and 50 stripes.

Head type	Head A		Head B	
# of stripes	25 stripes	50 stripes	25 stripes	50 stripes
Max. coating speed (mm/s)	14	7	20	20
Avg. width (μm)	217	289	178	176
Avg. thickness (nm)	102	158	92	101
Inter-stripe width non-uniformity (%)	11	19.3	11.8	13.6
Inter-stripe thickness non-uniformity (%)	9.8	11.3	8.7	12.8

156 mm × 2 mm, coating gap: 1 μm–35 mm with a resolution of 1 μm), vacuum dry unit (5×10^{-4} Torr), tension and motion controller for the web (web speed: 0.1 mm/s ~ 100 mm/s), syringe pump system (11 Elite I/W Single, Harvard Apparatus, 0.18 μl/min ~159.8 ml/min), O_3 plasma treatment (0.3 kW), and ionizers. An aqueous organic material, poly(3,4-ethylenedioxythiophene):poly(4-styrenesulfonate) (PEDOT:PSS, Clevios AI 4083), was coated on a 170-mm-wide PET film roll with the effective coating width of 150 mm. As a wetting agent, we added a 0.2 wt% fluorosurfactant into the pristine PEDOT:PSS solution. The viscosity (μ) and surface tension (σ) of the PEDOT:PSS solution are 6 mPa s and 21.32 mN/m, respectively. Before coating, we used a cellulose acetate disposable syringe filter (0.2 μm, DISMIC-25CS) to filter out aggregated particles existing in the PEDOT:PSS solution. The meniscus near the μ-tip was observed by an area scan camera (acA1300-30 gm, BASLER). The coated films were pre-dried in the vacuum dry unit for 10 min and hard-baked on a hot plate at 80 °C for 20 min. The surface roughness of slot-die heads and the profiles (width and thickness) of coated stripes were measured by 3D optical surface profiler (NV 6300, ZYGO).

To demonstrate the potential application of fine stripe coatings in OLED displays, we also fabricated OLED stripes using those slot-die heads. To this end, we fabricated the electrode (anode) stripes on the PET film roll using the conductive PEDOT:PSS (Clevios PH 1000) solution (Fig. 2(a)). To enhance its conductivity, we doped 5 wt% dimethyl sulfoxide (DMSO) into the pristine solution [17,18]. Using the DMSO-doped PEDOT:PSS solution, the contact pad was coated by the slot-die head with the shim only used for large-area coatings (coating width of 150 mm). The PET film with the PEDOT:PSS electrode stripes was attached to a carrier glass and loaded into an organic evaporator. We fabricated a phosphorescent green OLED (Fig. 2(b)) that consists of 15-nm-thick KHI-001 (Duksan Neolux) for a HIL, 40-nm-thick KHT-001 (Duksan Neolux) for a HTL, 15-nm-thick 4,4′-bis(N-carbazolyl)-1,1′-biphenyl (CBP) for an emission layer (EML), 10-nm-thick 4,7-diphenyl-1,10-phenanthroline (Bphen) for a hole/exciton blocking layer (HBL), 30-nm-thick LG-201(LG Chem., Ltd.) for an electron transport layer (ETL), 1-nm-thick lithium fluoride (LiF) for an electron injection layer (EIL), and 100-nm-thick aluminum (Al). In the green-emitting layer, 8 wt% *fac*-tris(2-phenylpyridine)iridium ($Ir(ppy)_3$) was doped. All the layers were deposited sequentially at a rate of 0.5 nm/s under a base pressure of 2×10^{-6} Torr by thermal evaporation.

2.2. Simulation method

To simulate and analyze the fluid dynamics in slit channels in the presence of scratches on the slot head surface, we used the CFD tool (ANSYS Fluent 19.1Ver.). It can track the shape and position of the interface using the volume of fluid (VOF) method and solving the Navier–Stokes equations describing the motion of the flow [19,20]. The geometry for simulations is presented in Fig. 3. To reduce the computational efforts, 2D structure with the computational area as large as 25 μm × 120 μm was considered with the gravity set. The width (25 μm) of the slit channel corresponds to the shim thickness. The total

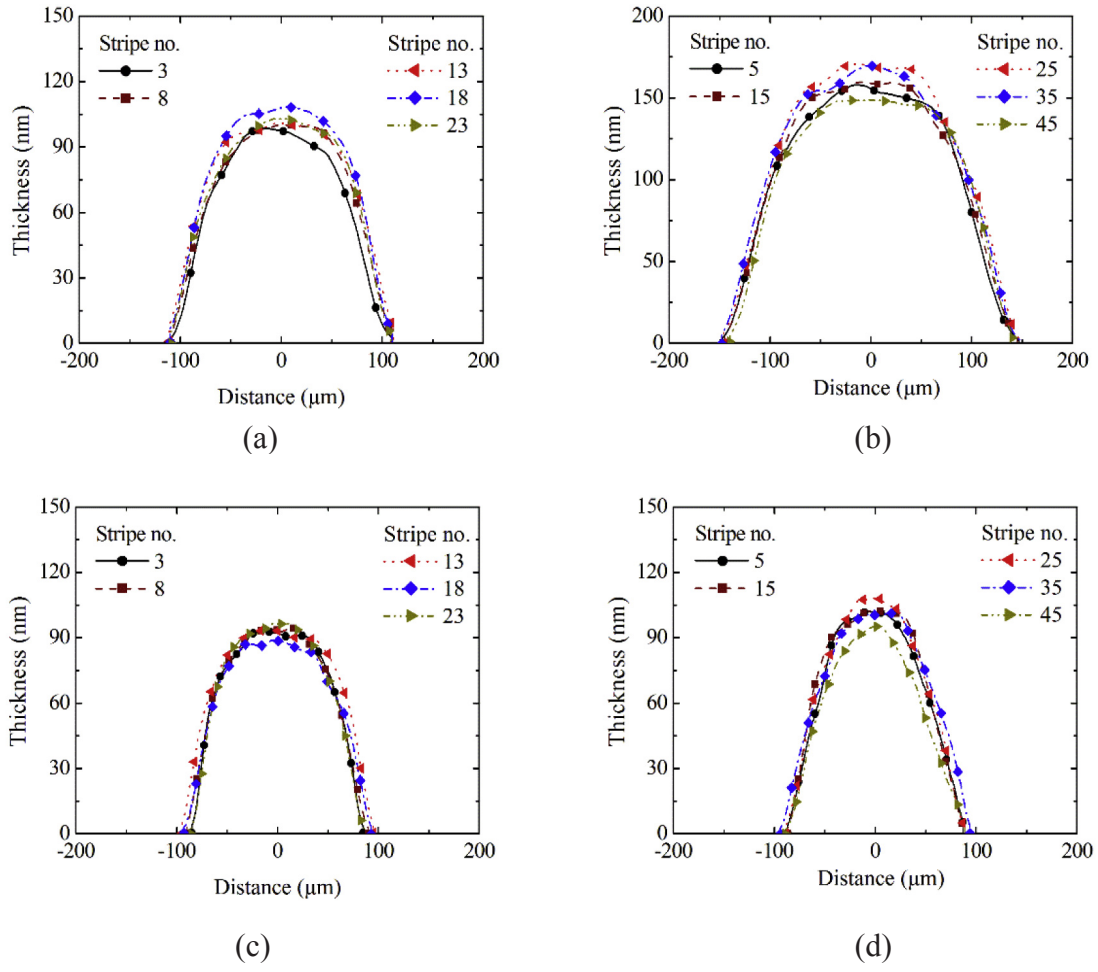

Fig. 7. Measure profiles of (a) 25 stripes and (b) 50 stripes coated using Head A, and (c) 25 stripes and (d) 50 stripes using Head B under the process condition in Table 1.

Table 4
Success or failure of 100 stripe coatings for different coating conditions.

Head type	Head A					Head B				
Shim thickness (μm)	50	50	25	25	100	50	50	25	25	100
μ-Tip length (μm)	500	250	500	250	250	500	250	500	250	250
Success (o)/failure (×)	×	×	×	×	×	×	o	×	o	×
Max. coating speed (mm/s)	–	–	–	–	–	–	14	–	14	–
Avg. width (μm)	–	–	–	–	–	–	229	–	227	–
Avg. thickness (nm)	–	–	–	–	–	–	100	–	103	–

number of meshes was 5810 (the minimum Δx was 0.48 μm). The boundary conditions for inlet, outlet, and walls were defined. The inlet was defined as a velocity-inlet and the outlet as outflow. The flow velocity (V) at the inlet was calculated by the formulation, Q/A, where Q is the volumetric flow rate and A the cross-sectional area of the slit channel. The computational area was initialized only with air. At the walls, the no slip condition was assumed due to the fact that the fluid in contact with the walls is stationary. The contact angle at the walls was set to be 15°. In fact, the contact angle (15°) of the PEDOT:PSS solution dropped on the surface of the slot-die head was measured to be almost the same as that (16°) on the surface of the meniscus guide. Finally, the physical models were selected. Two-phase air-liquid flow dynamics was simulated using the finite volume method. The flow of liquid was viscous laminar because the Reynolds number ($=\rho VD/\mu$, where ρ indicates the fluid density ($\approx 1000\,kg/m^3$), D the characteristic distance ($=25$ μm), and μ the fluid viscosity ($=6$ mPa s)) representing the ratio of inertial forces to viscous forces was as low as 0.0167. Therefore, the turbulent flow was not accounted for. The time step Δt ($=1$ μs) was calculated with a Courant Number equal to 0.25. The shape of scratches was assumed to be round and their radius was determined based on the measured surface roughness of the slot-die head.

3. Results and discussion

We have measured the surface morphology of those slot-die heads (Head A and Head B) used for fine stripe coatings. The measurements were carried out at 8 points within the region between the cavity and die lip where the fluid actually flows (Fig. 4). The optical images of their surfaces and measured surface profiles are presented in Fig. 5 and the surface roughness values are summarized in Table 2. In areas without scratches, the average (R_a) and peak-to-peak roughness (R_{pv}) values of Head A are measured to be as low as 3.6 nm and 0.06 μm, respectively. In local areas with scratches, however, R_a increases up to 19 nm and R_{pv} up to 3.5 μm. There appear short and long scratches in random directions, which are hardly seen to the naked eye. Meanwhile, Head B with uniformly rough surface shows the R_a value as high as 22 nm and the R_{pv} value of 2.8 μm. Although no scratches are observed in Head B, its surface morphology is as poor as that of Head A with local scratches (Table 2). It is noted that since a pair of the shim and meniscus guide is used in both Head A and Head B, the only difference

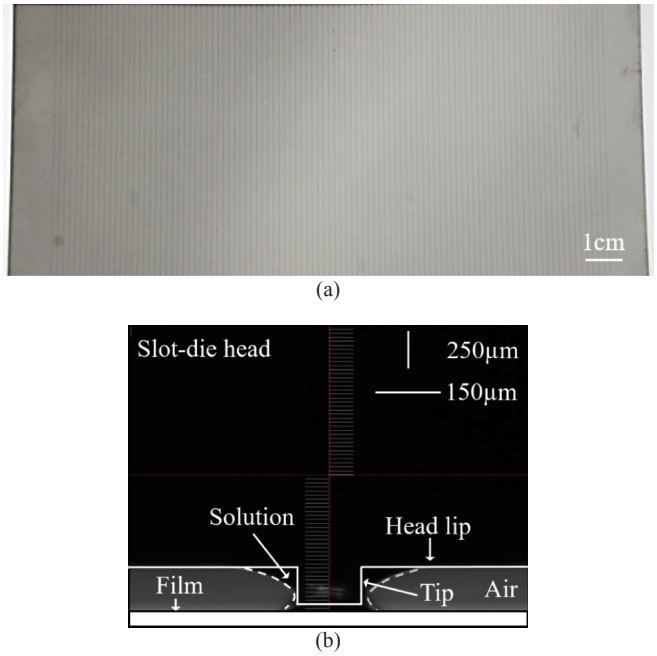

Fig. 8. (a) Image of 100 stripes without defects coated at 14 mm/s using Head B (25-μm-thick shim and 250-μm-long tips) and (b) flow distribution near the μ-tip captured by a vision camera.

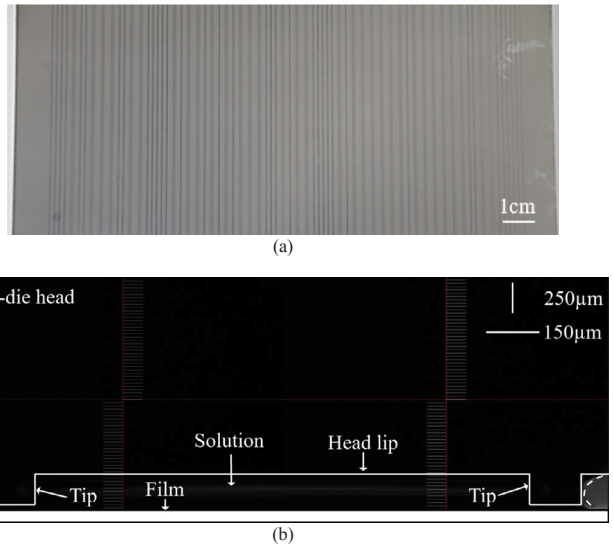

Fig. 9. (a) Image of 100 stripes with defects (line merging) coated at 7 mm/s using Head B (25-μm-thick shim and 250-μm-long tips) and (b) flow distribution near the adjacent μ-tips captured by a vision camera.

between them is the surface morphology.

To investigate the coating behaviors of those slot-die heads, we have first coated 25 and 50 stripes under the process condition in Table 1. To achieve narrow stripes, slot coatings were performed at a maximum coating speed, beyond which line breakup occurs. Shown in Fig. 6 are the images of coated stripes captured by a digital camera. It is evident that they are very straight. As summarized in Table 3, the maximum coating speed with Head B is as high as 20 mm/s. Using Head A, however, it is reduced to 14 mm/s for 25 stripes and further to 7 mm/s for 50 stripes. The coating speed with Head A is inevitably reduced to avoid line breakup. Such line breakup with Head A occurs at a relatively low speed due to scratch-induced unstable fluid flow through some slit channels. We will return to this point later with simulation results. We have measured the profiles of those stripes and presented

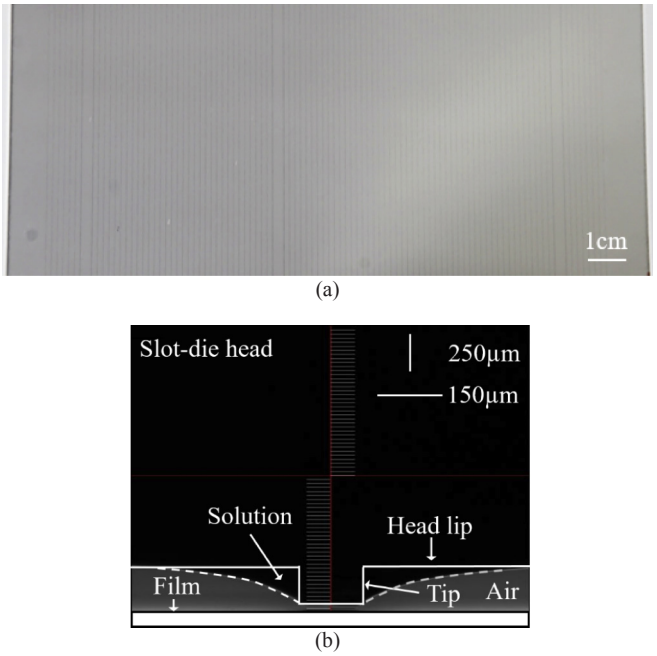

Fig. 10. (a) Image of 100 stripes with defects (line breakup) coated at 16 mm/s using Head B (25-μm-thick shim and 250-μm-long tips) and (b) flow distribution near the μ-tip captured by a vision camera.

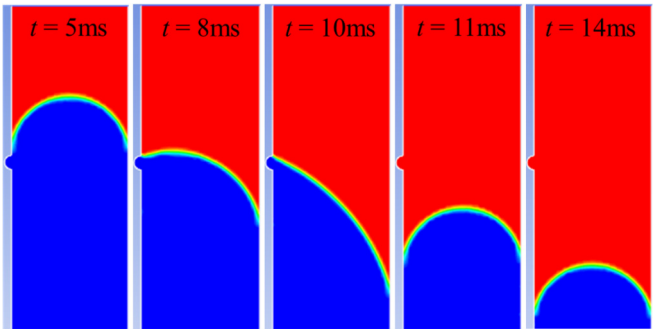

Fig. 11. Simulation results of transient phase distribution (liquid: upper red, air: lower blue) inside the slit channel in the presence of a single scratch (radius = 1.5 μm).

the results in Fig. 7 and Table 3. To quantify the film quality, we have measured the inter-stripe width and thickness non-uniformity, defined as (maximum width (thickness) – minimum width (thickness))/average width (thickness). The average width (176–178 μm) of 25 and 50 stripes coated using Head B is close to the μ-tip width (150 μm). Using Head A, however, it is much wider than the μ-tip width due to the reduced coating speed. Consequently, the average thickness of those stripes coated using Head A is observed to be high. As the number of stripes increases from 25 to 50, both slot-die heads show the degradation of the inter-stripe width and thickness uniformities. It is likely that the uniformity of the pressure distribution along the cavity is degraded as the number of outlets (μ-tips) increases. This phenomenon would also be observed if the shim defining the feed slot width is thick. In these cases, it is natural that the inter-stripe width and thickness uniformities are degraded because more fluid would flow through those μ-tips located in the middle of the slot-die head where the inlet is also positioned. Meanwhile, a sharp decrease in the inter-stripe width uniformity is observed with Head A. It implies that the effect of the surface morphology of the slot-die head becomes more pronounced with increasing number of stripes.

We have further fabricated 100 PEDOT:PSS stripes using those slot-

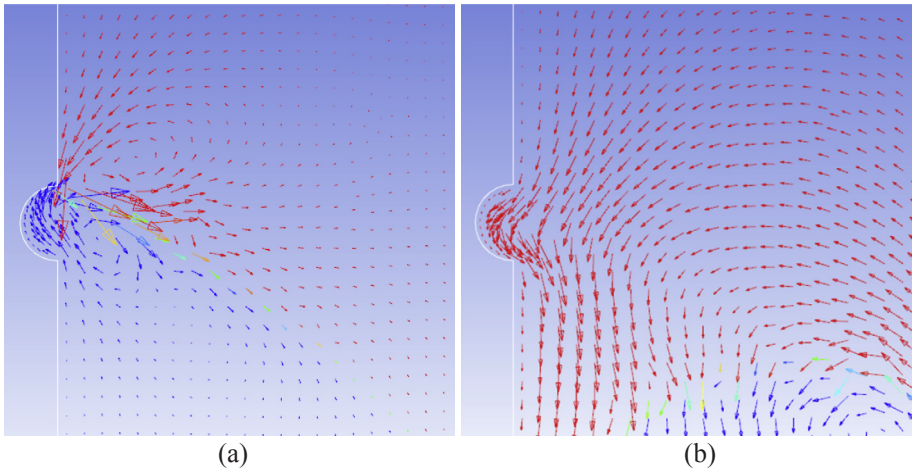

Fig. 12. Simulation results of transient velocity vector (liquid: red arrows, air: blue arrows) in the vicinity of a scratch (radius = 1.5 μm) at (a) t = 10 ms and (b) t = 10.74 ms.

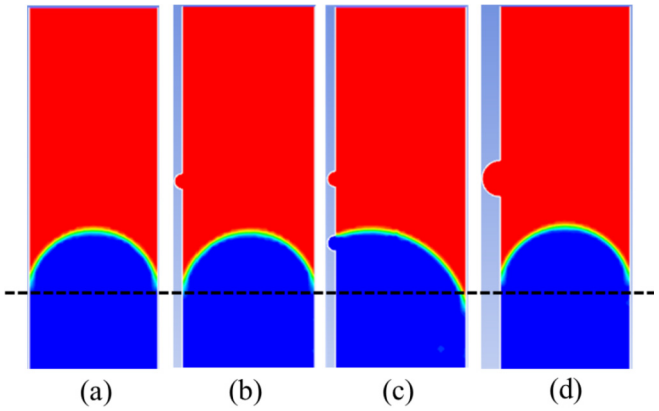

Fig. 13. Simulation results of transient fluid flow along the slit channel (a) without any scratch, (b) with a single scratch (radius = 1.5 μm), (c) with two scratches (radius = 1.5 μm), and (d) with a single scratch (radius = 3.5 μm) at t = 11 ms.

die heads with 100 μ-tips. The success or failure of stripe coatings is summarized in Table 4. Since μ-tips are placed more closely (Table 1) and the viscosity of the solution is low, the probability of occurrence of line merging is high [21]. At the same time, the probability of occurrence of line breakup is also high because the uniformity of the pressure distribution inside the cavity would be degraded with increasing number of outlets (μ-tips). If defects (line breakup and/or line merging) are observed, the coating was considered to be a failure. We can see in Table 4 that the success or failure of stripe coatings depends sensitively on the configurations of the shim and meniscus guide. Using Head B, 100 stripe coating without defects was feasible by reducing the shim thickness and μ-tip length, as evident in Fig. 8(a) showing the image of 100 stripes coated at 14 mm/s with the 25-μm-thick shim and 250-μm-long μ-tips. It is attributed that the uniformity of the pressure distribution along the cavity is enhanced by a thin shim and a resistance to flow from outlets to substrate is reduced by a short μ-tip. The average width of 100 stripes is increased to 227–229 μm because the coating speed is reduced to 14 mm/s (from 20 mm/s for 25 and 50 stripes) (Table 4). Presented in Fig. 8(b) is the flow distribution near the μ-tip captured by the area scan camera. The dashed line indicates the PEDOT:PSS solution distributed along the die lip and μ-tip, and the dark gray areas (below the dashed lines) represent the air gap between the die lip and film. It is clearly seen that the μ-tip controls the flow distribution and thus the stripe width. As shown in Fig. 9, however, defects (line merging) appear when coating at 7 mm/s using Head B with the same configuration (250-μm-long tips and 25-μm-thick shim). At a lower coating speed, line merging occurs because the fluids from the adjacent outlets would merge together on the head lip and flow along the μ-tips without separation (Fig. 9(b)). Meanwhile, there appears line breakup when the coating speed is 16 mm/s (Fig. 10). At a higher coating speed, the air gap (dark gray) in Fig. 10(b) appears inwards from μ-tip edges, implying that the fluid is not spread over the entire tip and eventually line breakup occurs.

Head A enables slot coatings of 25 and 50 stripes without defects, but not 100 stripes coatings (Tables 3 and 4). Unlike Head B, defects appear even if we reduce the μ-tip length and shim thickness of Head A. From this result, it is apparent that the effect of scratches is more pronounced with increasing number of stripes (μ-tips). To visualize their effects on the fluid dynamics, we performed simulations of the geometry (a slit channel with single or multiple scratches) in Fig. 3, which is based on the slot-die head with 100 μ-tips (μ-tip width of 150 μm and shim thickness of 25 μm). In this case, the flow velocity through a single slit channel is as low as 0.004 m/s (Q/A, where Q = 0.001 ml/min (=0.1/100 ml/min) and A = 25 μm × 150 μm). From the measured surface roughness values in Table 2, we have chosen the radius of the round-shaped scratches to be 1.5 μm or 3.5 μm. Presented in Fig. 11 is the transient phase (liquid-air two-phase) distribution inside the slit channel in the presence of a single scratch (radius = 1.5 μm). The parabolic distribution of the red liquid phase is due to the hydrophilic property (the contact angle of 15°) of the walls. Such a parabolic distribution is not maintained when the fluid encounters the scratch. While the fluid flows continuously along the wall without the scratch, the fluid flowing along the wall with the scratch is almost stationary for a short time. Namely, the continuous fluid flow is interrupted by the scratch as it cuts off the path along which the fluid can flow. Such a non-parabolic distribution of the liquid phase brings in a change in the distribution of the air phase. In the vicinity of scratch, we can see from Fig. 12(a) that the air velocity vector (blue arrows) is countercurrent to its main flow direction (downward), which increases a resistance to fluid flow and in turn changes the fluid flow to the lower right direction. When the liquid flows out of the scratch, the vortex flow or localized swirling is not observed, as evident in Fig. 12(b). It is attributed that the momentum of the fluid is very low in the vicinity of the scratch due to its low velocity. As such, the fluid flows down the horizontal face of the scratch and continues on its way. Around t = 11 ms, the parabolic distribution is recovered (Fig. 11).

We have further investigated its effect by increasing the number or size of scratches. Presented in Fig. 13 is the simulated transient phase distribution in the presence of two scratches with the radius of 1.5 μm and a single scratch with the radius of 3.5 μm. To roughly estimate the

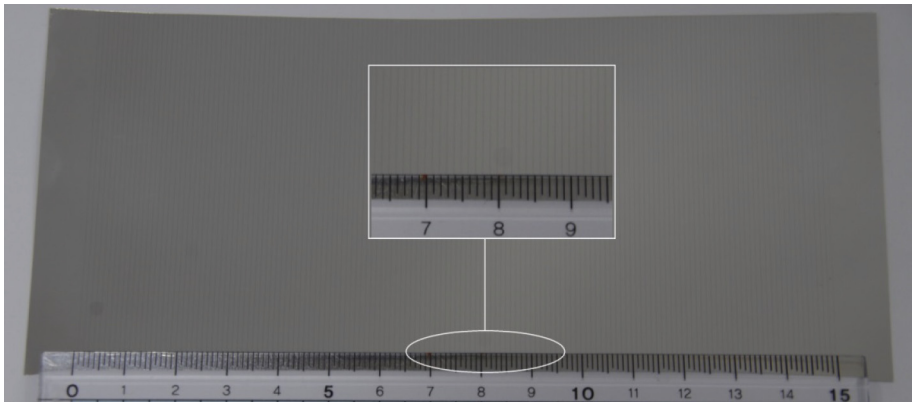

(a)

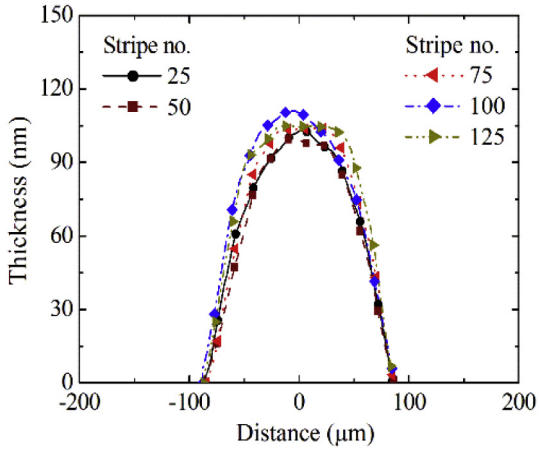

(b)

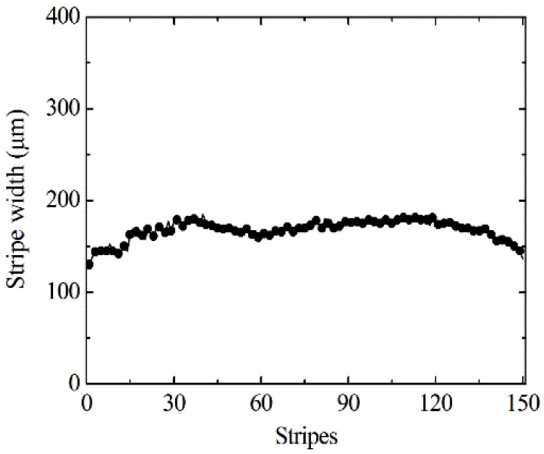

(c)

Fig. 14. Images of 150 stripes coated at 20 mm/s using Head B, (b) measured profiles of those stripes for different positions, and (c) measured width of each stripe.

velocity of fluid flow, we have placed the dash line in the figure. We can see that the fluid flows more slowly through the slit channel with a larger scratch. Since the flow velocity is inversely proportional to the cross-sectional area of the slit channel, the presence of scratches has the effect of increasing the average slit channel width. Such phenomena would cause the non-uniform pressure distribution among slit channels and eventually line breakup during fine stripe coatings.

Using Head B with uniformly rough surface but no scratches, we can fabricate 100 stripes without defects by reducing the shim thickness and μ-tip length. To further investigate its coating behaviors, we make an attempt to fabricate 150 stripes. Using Head B with 150-μm-wide tips and 25-μm-thick shim, it was not feasible to fabricate 150 stripes when the μ-tip was as long as 250 μm. It seems that a resistance to flow along the 250-μm-long tip is still too high. To reduce it, we shortened the μ-tips down to 150 μm. As evident in Fig. 14(a), we can fabricate 150 stripes even at the maximum coating speed of 20 mm/s. When the

Table 5
Measured width, thickness, and uniformity of 100 and 150 stripes coated using Head B with different μ-tip lengths.

Head type	Head B	
# of stripes	100	150
Shim thickness (μm)	25	
μ-Tip width (μm)	150	
μ-Tip length (μm)	250	150
Max. coating speed (mm/s)	14	20
Avg. width (μm)	227	168
Avg. thickness (nm)	103	103
Inter-stripe width non-uniformity (%)	9.2	32.8
Inter-stripe thickness non-uniformity (%)	6.8	10.7

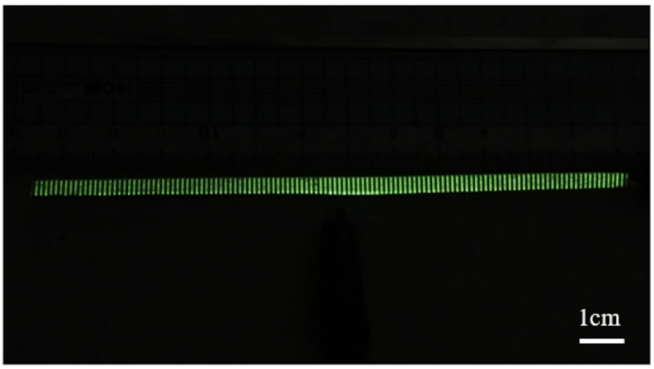

Fig. 15. Image of green light emission from 125 OLED stripes at 5 V.

μ-tip length was reduced from 500 μm (for 25 and 50 stripes) to 250 μm (for 100 stripes), the maximum coating speed was reduced from 20 mm/s to 14 mm/s (Tables 3 and 4) for stable coatings. In contrast, when the μ-tip length is reduced from 250 μm (for 100 stripes) to 150 μm (for 150 stripes), the maximum coating speed is rather increased from 14 mm/s to 20 mm/s (Table 5). For the μ-tip as short as 150 μm, the flow resistance is reduced to a great extent so that the amount of fluid reaching the substrate through the μ-tip is dramatically increased. As such, we can obtain 150 narrow stripes without reducing the coating speed (i.e., at 20 mm/s). Since the flow resistance is still high for the μ-tip with a length of 250 μm, we can obtain 100 stripes by reducing the coating speed to 14 mm/s. If the μ-tip length is properly chosen (< 250 μm), however, 100 stripes can also be achieved without reducing the coating speed (i.e., at 20 mm/s). We have measured the profiles of those stripes and presented the results in Fig. 14 (b)-(c) and Table 5. It is observed that although the average width (168 μm) is very close to the μ-tip width (150 μm), the inter-stripe width non-uniformity is as high as 32.8%, which is much higher than that (9.2%) of 100 stripes. From Fig. 14(c), it is found that the width of stripes located near the ends of the film is narrower than that of stripes in the middle. Some of them have the width narrower than the μ-tip width. As mentioned earlier, it is due to the fact that the uniformity of the pressure distribution along the cavity is degraded with increasing slot opening. This result is expected because the number of outlets (μ-tips) increased, but the shim thickness was kept unchanged. To further enhance the inter-stripe width uniformity, the cavity structure may need to be changed. In fact, the cavity was so narrow (2 mm) and straight as to ensure the uniform pressure distribution (Fig. 4). Since the width of stripes located near the ends of the film is narrower, however, a tilted cavity structure rather than a straight cavity structure may be required. Namely, the further away from the center of the slot-die head, the less the interval between the cavity and head lip. It may reduce the pressure difference between the end and the center of the slot-die head.

To demonstrate the potential application of R2R stripe coatings using the slot-die head (Head B) with μ-tips in AMOLED displays, we have fabricated fine OLED stripes. In reality, RGB stripes are coated on the active pixel area where indium-tin-oxide (ITO) is formed [9]. Since fabricating a pixelated ITO anode on the PET film roll is costly, we have coated the conductive PEDOT:PSS stripes on the PET film roll (Fig. 2(a)) using Head B with 150 μ-tips (width and length of 150 μm) and 25-μm-thick shim. Due to the limited size of vacuum chamber optimized for a 100 mm × 100 mm substrate, 125 OLED stripes were fabricated. As presented in Fig. 15, we have successfully obtained green light emission from those OLED stripes. Some dark spots are observed as they are not encapsulated. Furthermore, we can see the luminance difference between the center and the edge of the film because all the PEDOT:PSS anode stripes were connected to the single contact pad and the electrical contact was at the center of the pad. Even so, this experiment demonstrates the potential application of the proposed coating technology in solution-processable AMOLED displays.

4. Conclusion

Through CFD simulation and experimental validation of fluid flow in the slot-die head with meniscus-guiding μ-tips, we investigated the effect of its surface morphology on R2R slot coatings of fine PEDOT:PSS stripes. From CFD simulations, we found that the fluid velocity was reduced due to the effect of increased average slit channel width in the presence of scratches, possibly resulting in the non-uniform pressure distribution among slit channels. Accordingly, the success or failure of fine stripe coatings was affected by the surface morphology of the slot-die head and its effect was more pronounced with increasing number of stripes (μ-tips). It was not feasible to fabricate 100 stripes within the effective coating width of 150 mm using the slot-die head with good surface roughness (R_a = 3.6 nm) but local scratches (R_{pv} = 2.7 μm) due to scratch-induced unstable fluid flow in some slit channels. Using the slot-die head with uniformly rough surface (R_a = 22 nm) but no scratches, however, we fabricated 150 stripes without defects by reducing the μ-tip length to 150 μm (i.e., suppressing the flow resistance) and the shim thickness to 25 μm (i.e., enhancing the pressure distribution inside the cavity). We achieved fine stripes with the average width of 168 μm using 150-μm-wide μ-tips and the average thickness of 103 nm at 20 mm/s. We also fabricated OLEDs on the conductive PEDOT:PSS stripes and successfully achieved light emission from 125 OLED stripes, demonstrating the potential application of R2R stripe coatings using the slot-die head with meniscus-guiding μ-tips in solution-processable AMOLED displays.

Acknowledgement

This research was supported by Basic Science Research Program through the National Research Foundation of Korea (NRF) (NRF-2018R1D1A1B07042248) funded by the Ministry of Education.

References

[1] F.C. Krebs, Sol. Energy Mater. Sol. Cells 93 (2009) 394.
[2] R.R. Søndergaard, M. Hösel, F.C. Krebs, J. Polym. Sci. B Polym. Phys. 51 (2013) 16.
[3] M.S. Carvalho, H.S. Kheshgi, AlChE J 46 (2000) 1907.
[4] C.F. Lin, D.S. Wong, T. Liu, P. Wu, Adv. Polym. Technol. 29 (2010) 31.
[5] B. Park, O.E. Kwon, S.H. Yun, H.G. Jeon, Y.H. Huh, J. Mater. Chem. C 2 (2014) 8614.
[6] T.T. Larsen-Olsen, B. Andreasen, T.R. Andersen, A.P.L. Böttiger, E. Bundgaard, K. Norrman, J.W. Andreasen, M. Jørgensen, F.C. Krebs, Sol. Energy Mater. Sol. Cells 97 (2012) 22.
[7] A. Sandström, H.F. Dam, F.C. Krebs, L. Edman, Nat. Commun. 3 (2012) 1002.
[8] D. Deganello, Printing techniques for the fabrication of OLEDs, in: A. Buckley (Ed.), Organic Light-emitting Diodes (OLEDs): Materials, Devices and Applications, Woodhead Publishing Limited, Cambridge, UK, 2013, p. 360.
[9] R. Chesterfield, A. Johnson, C. Lang, M. Stainer, J. Ziebarth, Inf. Disp. 27 (2011) 24.
[10] T.J. Faircloth, J.G. Innocenzo, C.D. Lang, SID Symposium Digest 39 (2012) 645.
[11] H. Liu, W. Xu, W. Tan, X. Zhu, J. Wang, J. Peng, Y. Cao, J. Colloid Interface Sci. 465 (2016) 106–111.
[12] M. Singh, H.M. Haverinen, P. Dhagat, G.E. Jabbour, Adv. Mater. 22 (2010) 673.
[13] D. Soltman, V. Subramanian, Langmuir 24 (2008) 2224.
[14] F.C. Krebs, Sol. Energy Mater. Sol. Cells 93 (2009) 465.

[15] http://www.igt.jp/coatema/2016_08_Coatema_Overview.pdf.
[16] H. Kang, J. Park, K. Shin, Robot. Comput. Integrated Manuf. 30 (2013) 363.
[17] K. Fehse, K. Walzer, K. Leo, W. Lövenich, A. Elschner, Adv. Mater. 19 (2007) 441.
[18] S.I. Na, S.S. Kim, J. Jo, D.Y. Kim, Adv. Mater. 20 (2008) 4061.
[19] J.D. Anderson, Computational Fluid Dynamics: the Basics with Applications, McGraw-Hill Science, 1995.
[20] I. Lun, R.K. Calay, A.E. Holdo, Appl. Energy 53 (1996) 299.
[21] S.M. Raupp, M. Schmitt, A.-L. Walz, R. Diehm, H. Hummel, P. Scharfer, W. Schabel, J. Coating Technol. Res. 15 (2018) 899.